NANO LETTERS

Letter

pubs.acs.org/NanoLett

Connecting Metallic Nanoparticles by Optical Printing

Julián Gargiulo,[†] Santiago Cerrota,[†] Emiliano Cortés,[†] Ianina L. Violi,[†] and Fernando D. Stefani*[,†,‡]

[†]Centro de Investigaciones en Bionanociencias (CIBION), Consejo Nacional de Investigaciones Científicas y Técnicas (CONICET), Godoy Cruz 2390, C1425FQD Ciudad de Buenos Aires, Argentina

[‡]Departamento de Física, Facultad de Ciencias Exactas y Naturales, Universidad de Buenos Aires, Güiraldes 2620, C1428EAH Ciudad de Buenos Aires, Argentina

Supporting Information

ABSTRACT: Optical printing is a simple and flexible method to bring colloidal nanoparticles from suspension to specific locations of a substrate. However, its application has been limited to the fabrication of arrays of isolated nanoparticles because, until now, it was never possible to bring nanoparticles closer together than approximately 300 nm. Here, we propose this limitation is due to thermophoretic repulsive forces generated by plasmonic heating of the NPs. We show how to overcome this obstacle and demonstrate the optical printing of connected nanoparticles with well-defined orientation. These experiments constitute a key step toward the fabrication by optical printing of functional nanostructures and microcircuits based on colloidal nanoparticles.

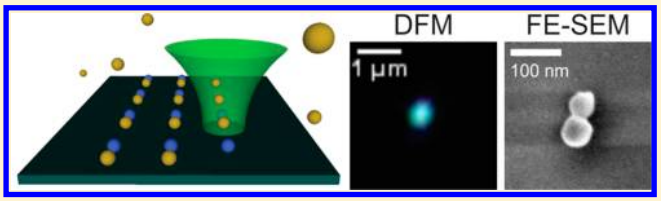

KEYWORDS: *Optical forces, gold nanoparticle, silver nanoparticle, laser tweezers, optical manipulation, thermophoresis*

Since recently, the use of optical forces to immobilize colloidal metal nanoparticles (NPs) one by one on specific locations of a substrate has been investigated.[1−7] In this method, called laser or optical printing, optical forces are applied to a colloidal nanoparticle in order to bring it close enough to a substrate so that the attractive force between the substrate and the particle dominates, and the nanoparticle gets fixed. Despite being an optical method, the positional accuracy of optical printing is not limited by diffraction of light, and individual NPs can be positioned with a precision of several tens of nanometers.[1]

In comparison to other nanofabrication tools, such as standard top-down methods, optical printing holds a number of advantages. First, colloidal chemistry offers an assortment of nanoparticles impossible to obtain with lithographic methods. Colloidal metallic nanoparticles can be prepared in a vast variety of compositions, sizes, shapes, structures (e.g., core−shell) and with numerous surface supramolecular modifications.[8−11] Also, colloidal nanoparticles typically have much higher crystal quality, which is critical for some applications, like plasmonics. Second, optical printing is fast and flexible and does not require high-cost instrumentation or clean rooms. Finally, there is no real limitation to extend optical printing to nonmetallic nanoparticles.

Optical printing was used to build complex surface-bound plasmonic nanostructures with high precision. After a first demonstration of direct printing of spherical gold NPs from colloidal suspension,[1,2] this methodology was applied to print aligned gold nanorods,[5] gold bipyramids,[7] and gold NPs holding DNA-origami structures.[6] Optical printing of multiple NPs in an ordered fashion is also possible using spatially modulated light fields.[4,12] Gold nanoparticles were also incorporated in photonic crystal cavities[13] and even biological cells[14] by optical printing.

In spite of its practicality and high potential, optical printing has been limited to the fabrication of ordered arrays of isolated NPs because, until now, it was not possible to print NPs close together in a controlled manner. In different experiments the minimum interparticle distance has been found to be restricted to about 300 nm.[3,4] This limitation has obstructed the use of optical printing to the fabrication of plasmonically coupled structures and circuits of connected NPs. In a workaround to this limitation, NPs were optically printed on a thermoresponsive polymer film, where they could be brought closer together upon contraction of the polymer film.[3] Still in this case the interparticle distance was limited to about 120 nm. Overcoming this limitation would tremendously expand the field of application of optical printing, enabling the rapid and flexible fabrication of functional nanostructures such as plasmonically driven nanostoves,[15] nanoantennas,[16] plasmonic optical tweezers.[17] It would also be possible to construct designed surface patterns for enhanced Raman spectroscopy and biosensing,[18] large structures of connected NPs such as "plasmonic polymers",[19] and even microcircuits based on NPs.

Here, we study systematically the optical printing of Au−Au and Ag−Au NP dimers. We show that the repulsive interaction that has prevented printing of NPs at close distances is produced by light interaction with the already printed NP. We propose an explanation in terms of thermophoretic repulsion. Selecting a printing wavelength that minimizes light interaction with the already printed NP, we were able to optically print Ag and Au NPs at all interparticle separation distances and connect them in Ag−Au heterodimers with well-defined orientation. This constitutes the first, fundamental step for the fabrication of more complex nanostructures by optical printing.

Received: November 6, 2015
Revised: January 5, 2016
Published: January 8, 2016

DOI: 10.1021/acs.nanolett.5b04542
Nano Lett. 2016, 16, 1224−1229

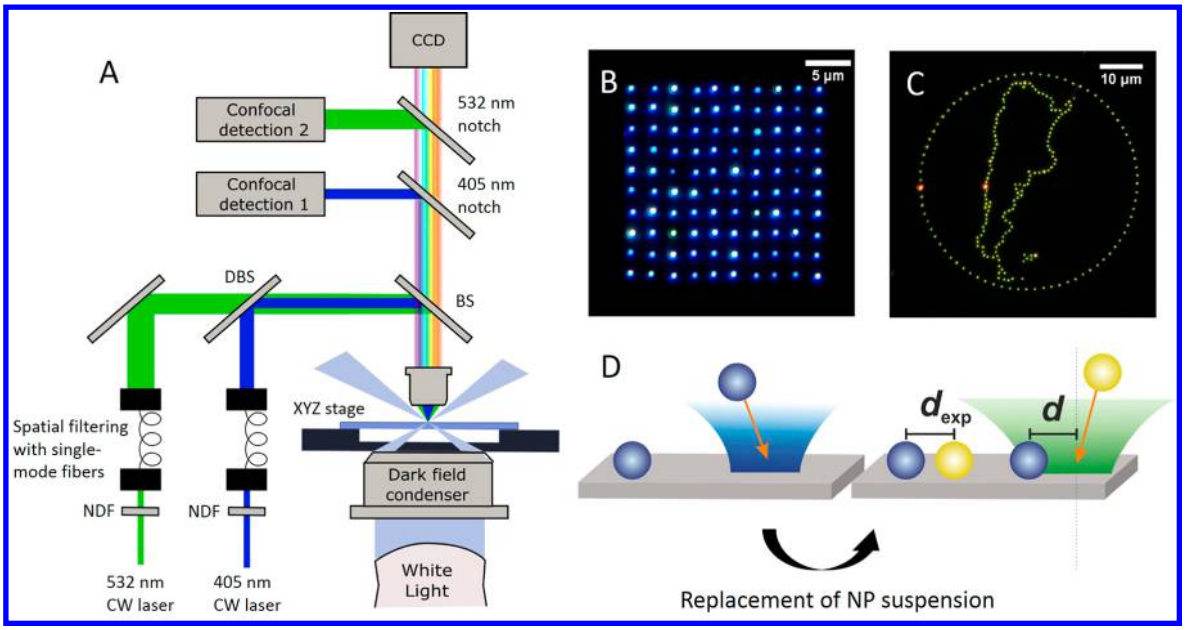

Figure 1. (A) Experimental setup; (B) A 10 × 10 grid of single 60 nm Ag NPs printed with the 405 nm laser, (C) A map of Argentina made of individual 60 nm Au NPs printed with the 532 nm laser; (D) Schematic of the process for dimers fabrication: first Ag NPs were optically printed with the 405 nm laser. Then the colloidal suspension is replaced by Au NPs, which are subsequently printed using the 532 nm laser. We define the interparticle separation set-point d as the distance between the center of the printed NP and the center of the printing laser focus (i.e., where the second NP should be printed). The achieved interparticle separation (center-to-center) is called d_{exp}.

The experimental setup is schematically depicted in Figure 1A. It consists of a home-built up-right optical microscope that combines dark-field detection in wide field and confocal sample scanning with CW lasers at 405 and 532 nm. These two lasers were used for optical printing as well. Both lasers were focused to their diffraction limit on the substrate plane and superimposed with a precision better than 10 nm in all three axes. Using notch filters, elastically scattered light was directed to respective amplified photodiodes through confocal pinholes. For dark-field imaging, the sample was illuminated with white light from an halogen lamp through an oil-immersion dark-field condenser (NA = 1.2−1.4). Scattered light was collected with a water immersion objective (NA= 1.0) and directed to a color CCD camera. With this configuration it is possible to simultaneously perform wide-field and confocal detections, which enables the automation and live monitoring of the printing process (see supporting info for more details).

Ag NPs, with an average size of 57 nm and a plasmon resonance centered at 428 nm, were printed using the 405 nm laser at 0.75 mW. Au NPs, with an average size of 63 nm and a plasmon resonance centered at 536 nm, were printed with the 532 nm laser at 1.2 mW. Both NPs were citrate coated, and negatively charged at neutral pH. For simplicity, and because the small difference in size is practically irrelevant for these experiments, 60 nm is used along the text for both NP sizes. In order to avoid spontaneous binding of the NPs, the substrates were surface functionalized with negative charges using layer-by-layer deposition of poly-electrolytes.[1] The focused laser beams generate optical forces on the NPs that push them toward the beam center and toward the substrate. Above a certain laser intensity the electrostatic repulsion from the substrate is surpassed and the NPs are printed.[1,4] The printing process was computer controlled and fully automated. Each printing event is detected as an increase in the scattered light signal on the corresponding confocal channel. Upon detection of a printing event, the laser illumination is immediately blocked, the sample is moved to the next printing position with a piezoelectric nanopositioning stage, and the laser is unblocked until the next printing event occurs. Additionally, a focus correction step could be included in between printing events when needed. Using this configuration, individual Ag and Au NPs were printed on arbitrary patterns with an average positional accuracy of 50 nm, a value 4 to 5 times better than the optical diffraction limit. Two examples are shown in Figures 1B and 1C.

We then turned to print dimers of NPs using the same setup configuration and the following procedure. First, a grid of NPs was printed as described above. Then, each dimer was fabricated with the following steps: (i) the position of a printed NP was determined, with a precision of approximately 1 nm, through a confocal scan using lower laser intensities for which no printing takes place, (ii) the piezoelectric was moved to the desired set-point d for the second NP, (iii) the laser intensity was increased to printing conditions until the printing of the second NP was detected, and (iv) a second confocal scan was performed to determine the relative position of the second NP. All these steps were automated via PC control. Further experimental details are provided in the Supporting Information. The set-point d is defined as the distance from the center of the printed NP to the center of the laser focus, i.e., where it is aimed to print the second NP.

Dimers of 60 nm Au NPs were fabricated by optical printing at 532 nm. Various set-points d of interparticle separation distances were used, ranging from 800 to 60 nm. In Figure 2A we show a set of Au NP dimers and in Figure 2D the average achieved interparticle distance d_{exp} versus the set-point d. For large separation distances (>300 nm) the printing process takes place smoothly, and the dimers can be fabricated according to design. At separations below 300 nm a deviation from the set-point toward larger separations is observed, concomitantly with a dramatic increase in the average waiting time for printing (Figure S2). Clearly, a repulsive interaction is preventing the second NP from being printed correctly. For separations smaller than 250 nm the repulsion is strong enough to completely prevent the printing of the second particle, and dimers cannot be

DOI: 10.1021/acs.nanolett.5b04542
Nano Lett. 2016, 16, 1224−1229

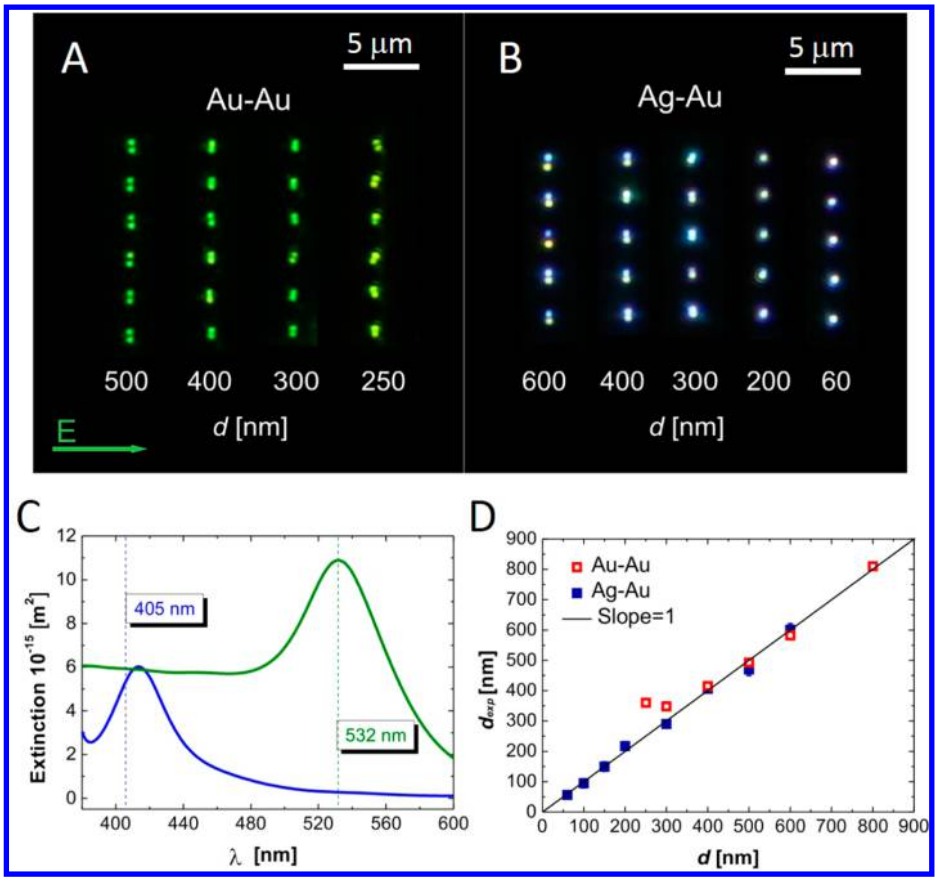

Figure 2. (A,B) Dark field micrographs of Au−Au and Ag−Au NP dimers fabricated at different interparticle distances *d*. (C) Extinction cross sections calculated using Mie theory for 60 nm Au and Ag NPs in water. (D) Measured interparticle distances (d_{exp}) vs set point (d) for the Au−Au and Ag−Au NP dimers. The ideal behavior is shown as a line with slope = 1.

fabricated. At this condition no printing event was observed even for waiting times 20-fold longer than the time needed to print at larger set-points.

The three different behaviors observed: no interaction, interaction with printing, and interaction without printing, are consistent with previous observations with 200 nm Ag NPs.[4] Printing Au−Au dimers with separations smaller than 300 nm has also been reported to be impossible.[3] Until now, two phenomena had been identified as potentially responsible for the minimum achievable interparticle distance: (i) optical interactions through the field scattered by both, the already printed NP and the NP in suspension (optical binding)[4] and (ii) convective flows induced by optical heating of the already printed NP.[3] All plausible mechanisms require interaction of the printed NP with light, either by scattering or absorption. One strategy to avoid these two effects consists of printing first a Ag NP, and then a Au NP using light of 532 nm (Figure 1D). In this way, printing of the Au NP is expected to take place undisturbedly, because the Ag NP is practically transparent at 532 nm (Figure 2C).

The fabrication protocol for Ag−Au dimers was analogous to the one used for Au−Au dimers. First a grid of 60 nm Ag NPs was printed using the 405 nm laser. Then the colloidal suspension was exchanged for one of 60 nm Au NPs. Finally the dimers were fabricated by a sequence of (i) a confocal scan at 405 nm to determine the exact position of the Ag NP, (ii) positioning the piezo stage at the desired printing position for the Au NP, (iii) illumination with 532 nm at printing intensity, and (iv) confocal scans to characterize the fabricated dimer. Figure 2B shows dark field images of Ag−Au heterodimers fabricated with various interparticle separation distances. Remarkably, in this case optical printing is possible for all interparticle distances. When the separation is smaller than the diffraction limit (<300 nm) the heterodimers appear as a single object in the dark-field images (Figure 2B). Nevertheless, using three confocal scattering images, one at 405 and two at 532 nm, with polarization perpendicular to the dimer axis, we were able to determine the positions of the Ag and the Au NPs with a subdiffraction precision of approximately 20 nm (more details in the Supporting Information).

The average interparticle distance achieved in the Ag−Au dimers is in agreement to the set-point (d) all the way down to 60 nm (Figure 2D), i.e. until the NPs are in contact. At this point is important to recall that aside from their optical properties, the Ag and Au NPs have practically identical physicochemical properties, such as size, charge and surface capping molecules. Based on this we conclude that the repulsive interaction that prevents the fabrication of Au−Au NP dimers with gaps smaller than 250 nm is light induced.

For the fabrication of structures and circuits of NPs, is not only important to control the interparticle distance and to be able to connect NPs, but also to control the relative orientation of the printed NPs with respect to the substrate/device frame of reference. We interrogated the possibilities of optical printing to fabricate dimers with controlled orientation. For this, we analyzed the angle (α) between the vertical axis (x) of the substrate and the vector defined from the center of Ag NP to the center of Au NP (see inset in Figure 3A).

Figure 3A shows the mean values of α for dimers fabricated at various interparticle distances d ranging from 600 to 60 nm,

DOI: 10.1021/acs.nanolett.5b04542
Nano Lett. 2016, 16, 1224−1229

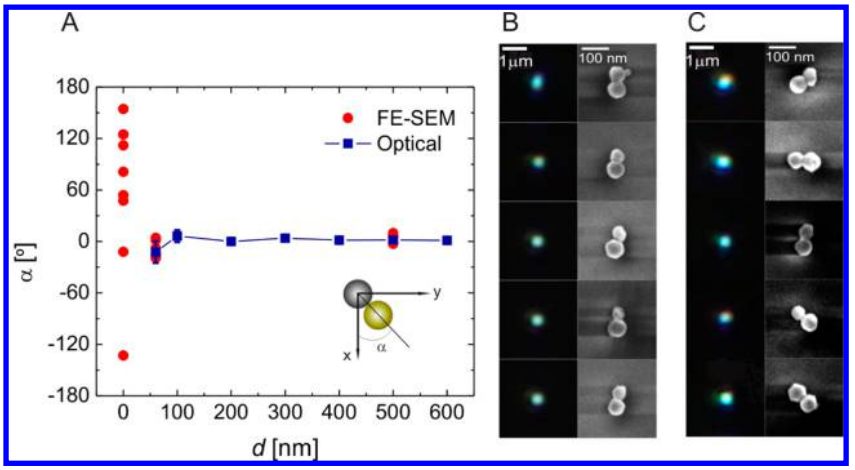

Figure 3. (A) Angle (α) between the vertical axis (x) of the substrate and the vector defined from the center of Ag NP to the center of Au NP. The optical measurement of α corresponds to the mean values obtained from analysis of confocal scattering images of at least 20 dimers for each value of d. Several values of α obtained from the analysis of FE-SEM images are shown for d = 500, 100, and 0 nm. (B, C) Dark field (left) and FE-SEM (right) images of Ag−Au heterodimers fabricated at d = 60 nm (B) and d = 0 nm (C). In B the Ag NPs is always the one on the top.

obtained from the analysis of confocal scattering images. The optical printing is accurate in terms of directionality within an error smaller than 8° for all values of d from 600 nm down to 100 nm. For the connected NPs (d = 60 nm), the variability takes a slightly higher value of 20°. There are two possible reasons for this increment. First, due to the limited printing accuracy, a larger variation in α is expected as d becomes shorter. Second, a contribution due to contact interactions between the NPs is also likely. As an example, in Figure 3B we show dark-field and field-emission scanning electron microscopy (FE-SEM) images of five connected Ag−Au NP dimers fabricated by setting the interparticle distance to 60 nm. On the dark field images the dimers appear as single diffraction limited scatterers. On the FE-SEM images the orientational control is evident. Ag−Au NP dimers can be fabricated as well if the interparticle distance is set to zero, but the orientational control is completely lost (Figure 3A,C).

These experiments clearly show that optical printing is capable of placing NPs at arbitrary separation distances and also connect NPs with controlled orientation. The necessary condition is to minimize the interaction of the already printed NPs with the light used for printing. In this case we achieved this by printing first a Ag NP using 405 nm light, and then a Au NP using 532 nm. Naturally, many other configurations that fulfill this condition can be thought of. However, designing an optimum strategy for the printing of connected NPs requires a deeper understanding of the light-induced repulsion.

The light-induced repulsive force that prevents optical printing of Au−Au dimers is active over relatively long distances (350−400 nm), which excludes near field interactions. Far field-interaction through dipolar fields scattered by the two NPs (the one already printed and the one being printed), so-called "optical binding",[4,20] is of second order (proportional to the square of the NP polarizability) and considerably weaker than the scattering force exerted by the laser on the NP being printed (first order on polarizability).[21] In addition, we have not observed any polarization dependency on the repulsion, as predicted by optical binding. We thus infer that some other, stronger repulsive force prevents the NPs approaching each other.

The other possibility to be considered is light absorption and heating. A repulsion explained in terms of convective flows in the surrounding fluid (water in our case) due to heating of the already printed NP is also inaccurate, for the following reasons. Even though metallic NPs are very efficient light-to-heat converters,[22] heat transfer to the surrounding medium is dominated by conduction[23] and convective flows are never faster than 1 nm/s. Such flows translate into drag forces of about 10^{-19} N, which are negligible in comparison to the printing forces.

We therefore propose an explanation based on thermophoretic forces product of the extreme temperature gradients generated around metallic NPs when they are illuminated at their plasmon resonance (Figure 4A). Thermophoresis is the movement of colloidal particles induced by temperature gradients.[24−26] In recent years, thermophoretic forces have proven to be strong enough for trapping and manipulation of nanometric sized objects[27,28] and have been found responsible for the motion of self-propelled Janus particles.[29]

The thermophoretic velocity V_{tph} is proportional to the temperature gradient:

$$V_{tph} = -D_T \nabla T \tag{1}$$

The thermodiffusion coefficient D_T is typically positive; i.e., particles move from hotter to colder regions, except for strongly charged colloids in solutions of high ionic strength and low temperatures.[30] The temperature increase at the surface of the printed NP ΔT_0 is proportional to the power absorbed by the NP. For a NP with absorption cross section σ_{abs} placed at a distance d from a Gaussian focused beam, the temperature increase can be expressed as (see SI):

$$\Delta T_0 = \frac{\sigma_{abs}}{2\pi^2 \kappa R} \frac{P}{w_0^2} e^{-2d^2/w_0^2} \tag{2}$$

where P is the total power of the beam, w_0 is the beam waist, R is the NP radius, and k is the thermal conductivity of the surrounding medium. The temperature increase around the NP is inversely proportional to the distance according to[15,22]

$$\Delta T(r) = \Delta T_0 R/r \tag{3}$$

Then it follows that the temperature gradient generated around a NP when it is illuminated by a Gaussian beam centered at a distance d from the NP is given by

$$\nabla T(r = d) = -\frac{\sigma_{abs} P}{2\pi^2 \kappa w_0^2 d^2} e^{-2d^2/w_0^2} \tag{4}$$

DOI: 10.1021/acs.nanolett.5b04542
Nano Lett. 2016, 16, 1224−1229

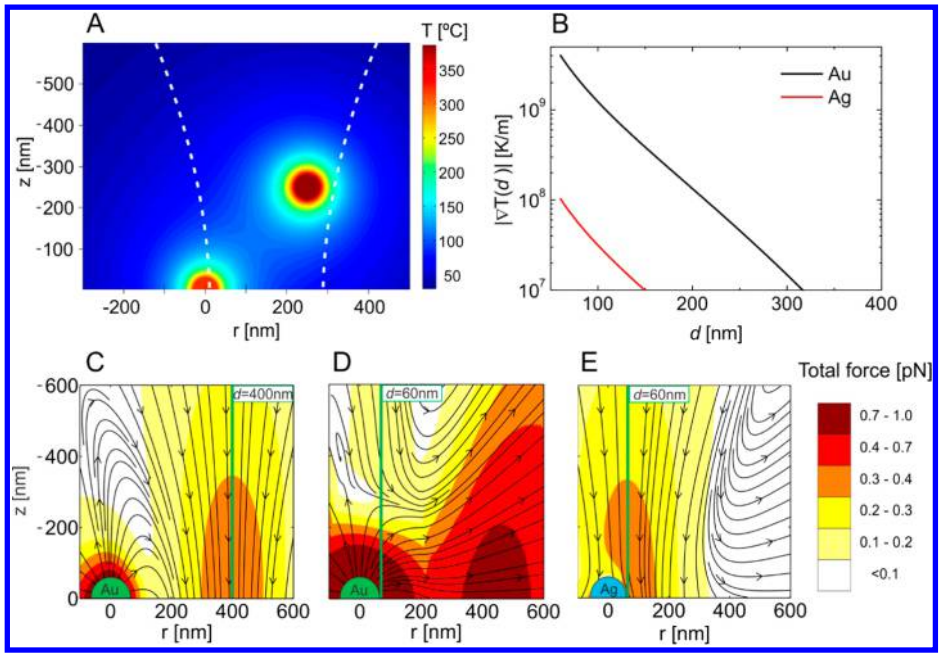

Figure 4. Temperature and forces generated by illumination of 60 nm Au and Ag NPs, located at (0,0) with a focused Gaussian laser beam of w_0 = 266 nm, λ = 532 nm, and P = 1.2 mW, as in the experiments. (A) Snapshot of the temperature field produced when a Au NP at (0,0) is approached by another Au NP at (250, 250) nm, that is being printed with the laser focus centered at d = 150 nm. (B) Temperature gradients evaluated at $r = d$ produced by a Au or a Ag NP at (0,0) as a function of the laser set point d. (C–E) Maps of total force (optical + thermophoretic) acting on a 60 nm Au NP for positions around a Au or Ag NP printed at (0,0), for different set points d of the laser focus. The arrows denote the direction of the resultant force and its magnitude is color coded. (C) printed NP of Au, d = 400 nm; (D) printed NP of Au, d = 60 nm; (E) printed NP of Ag, d = 60 nm. A thermodiffusion coefficient $D_T = 4.5 \times 10^{-11}$ m^2 s^{-1} K^{-1} was used. The immobilized NPs at (0,0) are drawn schematically with a diameter of 120 nm (i.e., two times their diameter) because calculations with interpenetrating NPs have no physical meaning.

The solutions of eq 4 for the cases of a 60 nm Au NP and a 60 nm Ag NP, and a focused Gaussian beam of 532 nm as the one used in the experiments, are shown in Figure 4B. The strong dependency of the generated temperature gradients with d, explains qualitatively the sharp transition from interacting without printing to correct printing behaviors for Au–Au dimers. The much smaller magnitude of the gradients produced by the Ag NP are consistent with the feasibility to fabricate Ag–Au dimers at arbitrarily close separations.

A quantitative comparison to the experiments requires the calculation of the thermophoretic force considering the temperature field produced by the two NPs (the one fixed at the substrate, and the one being printed). Using eq 1 and calculated temperature fields, it is possible to calculate the Stokes drag force:

$$F_{tph} = 6\pi R\mu V_{tph} \quad (5)$$

where viscosity of the suspension medium. Accurate experimental values of D_T are scarce in general, and to our knowledge not available for metallic particles. Estimating theoretically the value of D_T is not trivial and remains a challenging problem.[26,31] As reviewed by Piazza and Parola,[32] most of the measured coefficients range in the order of 10^{-12} to 10^{-11} m^2 s^{-1} K^{-1}. Typically, measurements of D_T involve temperature gradients 2–3 orders of magnitude weaker than the ones involved in our experiments and temperatures near room temperature.[30,33] The two experiments with the most similar conditions to our experiments are (i) the one performed by Bucholtz[34] et al. with laser-induced thermophoresis of silica microspheres in viscous liquids and (ii) the one with fullerenes in toluene performed by Bou-Ali et al.,[35] which is the only report involving heat conducting nanoparticles. The values of D_T obtained in those experiments were 2.2 × 10^{-11} m^2 s^{-1} K^{-1} and 4.5 × 10^{-11} m^2 s^{-1} K^{-1}, respectively. Here we show the calculations made with 4.5×10^{-11} m^2 s^{-1} K^{-1}.

We calculated the thermophoretic force produced on a Au NP at numerous positions around an already printed Ag or Au NP, for various positions d of the printing laser and including the temperature dependence of the viscosity of water. The optical force produced by the laser beam on the Au NP that is being printed was added to the thermophoretic force in order to obtain total force maps. In Figures 4C–E, three total force maps are shown. The force lines shown in Figures 4C–E can be interpreted as trajectories in the absence of Brownian motion. If the laser is relatively far from the printed NP, e.g., at 400 nm (Figure 4C), thermophoretic forces are negligible in comparison to the optical forces, and the printing path of the Au NP is practically undisturbed. As the laser gets closer to the printed Au NP and light absorption increases, the thermophoretic repulsive force becomes more important. For example for d = 60 nm (Figure 4D), thermophoretic repulsion dominates and printing is not possible at all. In contrast, if the printed NP is made of Ag (Figure 4E), the thermophoretic forces are significantly weaker even for d = 60 nm, and optical printing is possible at any interparticle separation. Further details on the optical forces and temperature calculations are included in the SI. It is remarkable that these simple calculations with no free parameter reproduce all experimental observations. To our knowledge there are no reported values of D_T for Au NPs, and for no kind of NP under such high temperature gradients. It is therefore interesting to explore the range of suitable values of D_T. We find that values ranging from 2×10^{-11} to 2×10^{-10} m^2 s^{-1} K^{-1} lead to calculated force fields compatible with the experimental observations. The best fit to the onset of repulsion observed on the fabrication of Au–Au dimers is obtained with a value of 8×10^{-11} m^2 s^{-1} K^{-1}.

DOI: 10.1021/acs.nanolett.5b04542
Nano Lett. 2016, 16, 1224–1229

In conclusion, we have shown that the limitation of optical printing to position NPs at close interparticle distances can be overcome by minimizing the interaction with light of the already printed NPs. This limitation has until now limited the application of optical printing to patterns of well separated NPs. Selecting a wavelength for which the printed Ag NP is practically transparent, we managed to fabricate Ag−Au NP dimers at any interparticle separation, as well as connected dimers with controlled orientation.

After an evaluation based on physical arguments and calculations of all plausible mechanisms, we conclude that the repulsion that has restricted the optical printing of close by NPs is due to thermophoresis. Light absorption by the already printed NP generates very large temperature gradients, which in turn produce strong thermophoretic repulsive forces.

The results presented on this paper expand dramatically the field of application of optical printing as a template-free and versatile nanofabrication strategy for positioning colloidal NPs on a solid surface. They constitute the fundamental step for the fabrication of complex functional nanostructures and circuits based on connected NPs. They also provide a clear guideline for devising new, optimized optical printing strategies fulfilling the key condition of avoiding light absorption by the printed NPs. For example, a viable strategy for metallic NPs would be to use substrates with high refractive index, so that the NP plasmon resonance red-shifts considerably when they pass from suspension to the substrate. Then the printing wavelength could be tuned so as to have minimum interaction with the printed NPs. Furthermore, we believe that optical printing can strongly benefit from a deeper comprehension of thermophoretic forces on (metal) nanoparticles. In particular, finding conditions for which the thermodiffusion coefficient reduces significantly or even changes sign, e.g., by modifying ionic strength,[30] would facilitate optical printing of connected alike nanoparticles.

■ ASSOCIATED CONTENT

Supporting Information

The Supporting Information is available free of charge on the ACS Publications website at DOI: 10.1021/acs.nanolett.5b04542.

Details about the materials, the preparation of substrates, the automation of the optical printing process, the determination of the printing times, the optical determination of interparticle distances, as well as for the calculations of optical and temperature fields (PDF)

■ AUTHOR INFORMATION

Corresponding Author

*E-mail: fernando.stefani@cibion.conicet.gov.ar.

Funding

This project was funded with the support of CONICET, ANCYPT projects PICT-20090110 and PICT-2010-2511, and a Partner Group of the Max-Planck-Society.

Notes

The authors declare no competing financial interest.

■ ACKNOWLEDGMENTS

F.D.S. would like to thank Alex Fainstein, Ernesto Calvo, Andrea Bragas, Oscar Martínez, Enrique San Román, Pedro Aramendía, and Lía Pietrasanta for their support with instrumentation and materials. J.G. would like to thank Alina Ghisolfi for the TOC and Abstract graphic.

■ REFERENCES

(1) Urban, A. S.; Lutich, A. A.; Stefani, F. D.; Feldmann, J. *Nano Lett.* **2010**, *10*, 4794−4798.
(2) Guffey, M. J.; Scherer, N. F. *Nano Lett.* **2010**, *10*, 4302−4308.
(3) Urban, A. S.; Fedoruk, M.; Nedev, S.; Lutich, A.; Lohmueller, T.; Feldmann, J. *Adv. Opt. Mater.* **2013**, *1*, 123−127.
(4) Bao, Y.; Yan, Z.; Scherer, N. F. *J. Phys. Chem. C* **2014**, *118*, 19315−19321.
(5) Do, J.; Fedoruk, M.; Jäckel, F.; Feldmann, J. *Nano Lett.* **2013**, *13*, 4164−4168.
(6) Do, J.; Schreiber, R.; Lutich, A. A.; Liedl, T.; Rodríguez-Fernández, J.; Feldmann, J. *Nano Lett.* **2012**, *12*, 5008−5013.
(7) Guffey, M. J.; Miller, R. L.; Gray, S. K.; Scherer, N. F. *Nano Lett.* **2011**, *11*, 4058−4066.
(8) Daniel, M.; Astruc, D. *Chem. Rev.* **2004**, *104*, 293−346.
(9) Xia, Y.; Xiong, Y.; Lim, B.; Skrabalak, S. E. *Angew. Chem., Int. Ed.* **2009**, *48*, 60−103.
(10) Murphy, C. J.; Sau, T. K.; Gole, A. M.; Orendorff, C. J.; Gao, J.; Gou, L.; Hunyadi, S. E.; Li, T. *J. Phys. Chem. B* **2005**, *109*, 13857−13870.
(11) Ghosh Chaudhuri, R.; Paria, S. *Chem. Rev.* **2012**, *112*, 2373−2433.
(12) Nedev, S.; Urban, A. S.; Lutich, A. A.; Feldmann, J. *Nano Lett.* **2011**, *11*, 5066−5070.
(13) Do, J.; Sediq, K. N.; Deasy, K.; Coles, D. M.; Rodríguez-Fernández, J.; Feldmann, J.; Lidzey, D. G. *Adv. Opt. Mater.* **2013**, *1*, 946−951.
(14) Li, M.; Lohmüller, T.; Feldmann, J. *Nano Lett.* **2015**, *15*, 770−775.
(15) Baffou, G.; Quidant, R. *Laser Photon. Rev.* **2013**, *7*, 171−187.
(16) Curto, A. G.; Volpe, G.; Taminiau, T. H.; Kreuzer, M. P.; Quidant, R.; van Hulst, N. F. *Science* **2010**, *329*, 930−933.
(17) Grigorenko, A. N.; Roberts, N. W.; Dickinson, M. R.; Zhang, Y. *Nat. Photonics* **2008**, *2*, 365−370.
(18) Wang, H.; Levin, C. S.; Halas, N. J. *J. Am. Chem. Soc.* **2005**, *127*, 14992−14993.
(19) Slaughter, L. S.; Willingham, B. A.; Chang, W.-S.; Chester, M. H.; Ogden, N.; Link, S. *Nano Lett.* **2012**, *12*, 3967−3972.
(20) Yan, Z.; Shah, R. A.; Chado, G.; Gray, S. K.; Pelton, M.; Scherer, N. F. *ACS Nano* **2013**, *7*, 1790−1802.
(21) Dholakia, K.; Zemánek, P. *Rev. Mod. Phys.* **2010**, *82*, 1767−1791.
(22) Coronado, E. A.; Encina, E. R.; Stefani, F. D. *Nanoscale* **2011**, *3*, 4042−4059.
(23) Donner, J. S.; Baffou, G.; McCloskey, D.; Quidant, R. *ACS Nano* **2011**, *5*, 5457−5462.
(24) Würger, A. *Rep. Prog. Phys.* **2010**, *73*, 126601.
(25) Epstein, V. P. S. *Eur. Phys. J. A* **1929**, *54*, 537−563.
(26) Michaelides, E. E. *Int. J. Heat Mass Transfer* **2015**, *81*, 179−187.
(27) Braun, M.; Cichos, F. *ACS Nano* **2013**, *7*, 11200−11208.
(28) Braun, M.; Würger, A.; Cichos, F. *Phys. Chem. Chem. Phys.* **2014**, *16*, 15207−15213.
(29) Jiang, H.-R.; Yoshinaga, N.; Sano, M. *Phys. Rev. Lett.* **2010**, *105*, 268302.
(30) Putnam, S. A.; Cahill, D. G.; Wong, G. C. L. *Langmuir* **2007**, *23*, 9221−9228.
(31) Giddings, J. C.; Shinudu, P. M.; Semenov, S. N. *J. Colloid Interface Sci.* **1995**, *176*, 454−458.
(32) Piazza, R.; Parola, A. *J. Phys.: Condens. Matter* **2008**, *20*, 153102.
(33) Helden, L.; Eichhorn, R.; Bechinger, C. *Soft Matter* **2015**, *11*, 2379−2386.
(34) Schermer, R. T.; Olson, C. C.; Coleman, J. P.; Bucholtz, F. *Opt. Express* **2011**, *19*, 10571−10586.
(35) Yue, A. S. *J. Cryst. Growth* **1977**, *42*, 542−546.

■ NOTE ADDED AFTER ASAP PUBLICATION

Due to a production error, this paper was published prematurely on the Web on January 14, 2015, before the text corrections were implemented. The corrected version was reposted on January 15, 2015.

DOI: 10.1021/acs.nanolett.5b04542
Nano Lett. 2016, 16, 1224−1229